J. MATER. CHEM., 1992, 2(2), 191–196

Magnetic Structure of Iron(II) Phosphate, Sarcopside, $Fe_3(PO_4)_2$

Joanne K. Warner,[a] Anthony K. Cheetham,[a] Anders G. Nord,[b] Robert B. Von Dreele[c] and Mohana Yethiraj[c]

[a] *Chemical Crystallography Laboratory, University of Oxford, 9 Parks Rd, Oxford OX1 3PD, UK*
[b] *Department of Structural Chemistry, Arrhenius Laboratory, S-106 91, Stockholm, Sweden*
[c] *LANSCE, Los Alamos National Laboratory, Los Alamos, NM 87545, USA*

$Fe_3(PO_4)_2$, sarcopside, displays unusual magnetic properties which have been investigated using time-of-flight powder neutron diffraction and magnetic susceptibility measurements. The structure contains chains of three edge-shared FeO_6 octahedra with two inequivalent iron sites, the central M(1) site possessing a fairly regular symmetry and smaller volume compared with the two distorted M(2) sites of the terminal octahedra. In the absence of an applied field, the compound orders antiferromagnetically, with the M(2) sites in each chain having opposite spin directions along the [100] direction, leaving the central M(1) cation frustrated with no net spin. Under applied magnetic fields of <0.7 T, two magnetic phase transitions are observed, a field-induced ferrimagnetic–antiferromagnetic transition at 38(1) K and an antiferromagnetic–paramagnetic transition at 44(1) K. At fields >0.7 T, only the bicritical transition from ferrimagnetic to paramagnetic is observed at 44(1) K.

Keywords: *Magnetism*; *Neutron diffraction*; *Powder diffraction*; *Rietveld analysis*; *Iron(II) phosphate*

The recent review of anhydrous iron phosphates and oxyphosphates by Gleitzer,[1] and the Fe–P–O phase diagram at 900 °C established by Modaressi *et al.*,[2] show the enormous scope available within this system for the investigation of the magnetic ordering as a function of structure and valence state. Measurements carried out on compounds in this system generally reveal antiferromagnetic transitions, although weak ferrimagnetism, frustration and spin canting have also been observed.[3–7] Previously, we have determined the magnetic structure of two phases of the mixed valence compound Fe_2PO_5, in which the face-sharing $Fe^{II/III}O_6$ octahedra are aligned ferromagnetically within chains but with opposite spin directions between chains.[8,9] To further our understanding of these Fe–P–O systems, we are now studying $Fe_3(PO_4)_2$, which adopts two structural forms, graftonite,[10] and its high-pressure modification, sarcopside.[11]

A series of transition-metal phosphates isostructural with the mineral sarcopside have been shown to possess some very interesting magnetic and site-ordering properties. The structure consists of chains of edge-shared octahedra, similar to those of olivine but with every fourth octahedron missing. This leaves a chain of three octahedra containing two unique cation sites, the central M(1) site possessing a fairly regular symmetry and smaller volume compared with the two distorted M(2) sites of the terminal octahedra[12] (Fig. 1). $Ni_3(PO_4)_2$ is readily formed in this structure[13] by solid-state reaction under atmospheric conditions, and $Fe_3(PO_4)_2$ forms under high-pressure hydrothermal conditions. A full range of solid solutions $(Ni_xFe_{1-x})_3(PO_4)_2$ can be prepared.[14] The two end members display antiferromagnetic ordering with transitions at 18 and 44 K, respectively. In this study we have used time-of-flight neutron powder diffraction to examine $Fe_3(PO_4)_2$, sarcopside, to refine the nuclear structure at 60 K and determine the nature of the magnetic ordering at 10 K.

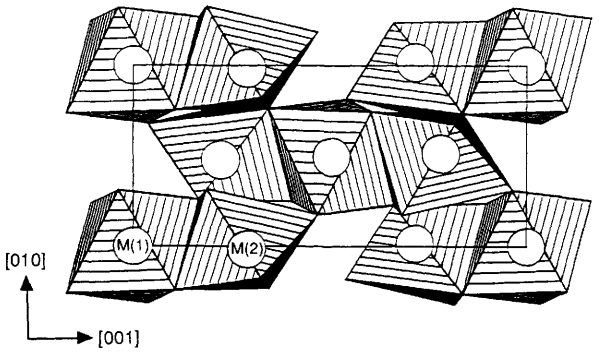

Fig. 1 The edge-shared FeO_6 octahedra in sarcopside, with the M(1) and M(2) sites depicted by circles

Experimental

A powder sample of iron sarcopside was prepared *via* a two-stage process involving a solution precursor. Stoichiometric quantities of $Fe(NO_3)_3 \cdot 9H_2O$ and $NH_4H_2PO_4$ were dissolved in distilled water and the solution heated to dryness in the fume cupboard. The resulting brown residue was slowly fired to 800 °C in a tube furnace with 10% H_2 in N_2 gas flowing, to complete the denitration and reduce the iron to form divalent $Fe_3(PO_4)_2$, graftonite. The pale cream powder was checked for purity by X-ray diffraction and was found to be highly crystalline. The sarcopside phase was prepared by sealing this material in gold tubes and heating them in a hydrothermal Nimonic-105 autoclave at 800 bar, 570 K for 7 days. The final product was found to be pure and of excellent crystallinity.

Low-temperature time-of-flight neutron powder diffraction data were collected with a 0.5 g sample on the high-intensity powder diffractometer, HIPD, at LANSCE, Los Alamos. Data from the 153, 90 and 40° detector banks were used in the analysis, covering a range of *d*-spacings of 0.4–14 Å. The sample was mounted in a 1/4″ diameter vanadium can, cooled by a Displex closed-cycle refrigerator. Data were collected at 10.1(1) K and above the magnetic transition ($T_N = 44$ K) at 59.7(1) K, for around 2 h each, and normalised to the incident spectral intensity.

Results

Nuclear and magnetic structure refinements were performed by the Rietveld[15] profile technique using GSAS,[16] as modified for magnetic refinements. The nuclear structure of $Fe_3(PO_4)_2$, sarcopside, was refined in space group $P2_1/c$ using the 59.7 K data set, and the parameters obtained were used as the basis

of the 10.1 K structure refinement. To avoid excessive correlation between the refined magnetic moment and the absorption correction, the absorption values obtained from the 59.7 K data were held constant in the 10.1 K refinement. The magnetic form factor for Fe^{2+} was calculated from the Hartree–Fock atomic wavefunctions[17] using the Cambridge Crystallographic Subroutine Library.[18]

In the low-temperature profile, all the peaks observed were consistent with the nuclear symmetry, but increased intensity was found in some reflections as a result of the magnetic scattering, with the strongest contribution to the (011) reflection. The (102) reflection displays considerable magnetic intensity, whilst having almost no nuclear contribution at 60 K. The possible collinear models for antiferromagnetic, ferrimagnetic and ferromagnetic structures were tested with a variety of spin directions. The three antiferromagnetic models are illustrated in Fig. 2.

The first model produced a number of reflections that are systematically absent in the observed pattern, and in particular a strong (010) reflection. It seems unlikely that any collinear arrangement of spins could produce the conditions in the structure-factor calculation that would remove intensity from all of these 'additional peaks', and this model was rejected. The second model is in many ways the most appealing, as the magnetic structure obeys the nuclear symmetry of $P2_1/c$. The inter- and intra-chain antiferromagnetic ordering would appear to offer strong exchange interactions and a stable magnetic configuration. The major limitation of this model is its failure to reproduce strong magnetic intensity in the (011) reflection without also giving greater intensity to other observed reflections. No single spin direction could reproduce the observed profile, and a variety of non-collinear orientations for the M(1) and M(2) sites were also examined and each model was tested with a variety of spin directions. By contrast, model (iii) gave convincing agreement with the observed data, with R_{Mag} of *ca.* 11%, compared to *ca.* 30% for other two. The optimum spin direction was found to be parallel to the *a* axis. Components refined for the *b* and *c* directions were found to be statistically insignificant and were fixed to zero.

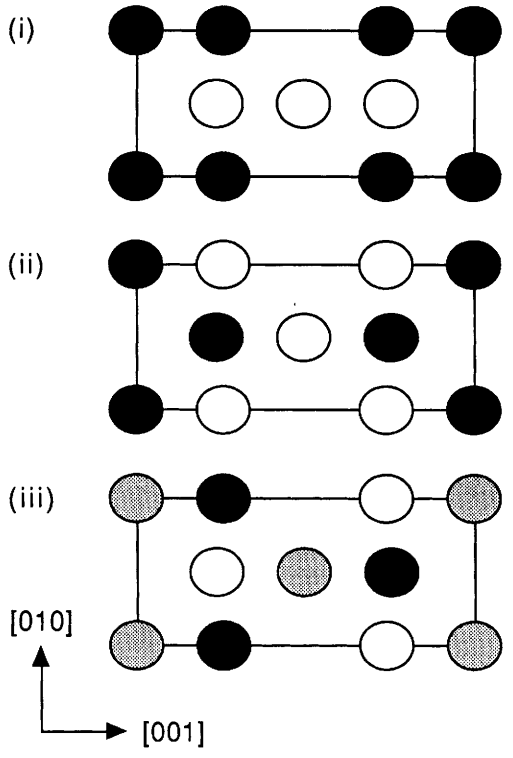

Fig. 2 Projection down [100] showing the possible collinear arrangements of spin on the M(1) and M(2) sites for antiferromagnetic ordering of Fe^{2+}. The black and white circles indicate opposing spin directions in the *ac* plane. The grey circles have no net spin

An average refined moment of $4.31(2)\mu_B$ was found for M(2), with no net moment on M(1) from the zero-field neutron powder diffraction data. Measurements using a Cryogenic S600 SQUID susceptometer between 6 K and room temperature with an applied field of 0.005 T show two magnetic transitions in this temperature range: a paramagnetic–antiferromagnetic transition at $T_N = 44(1)$ K, $\theta = -67(2)$ K, and what appears to be a field-induced spin–flop transition at 38(1) K (Fig. 3). The magnetic moment of Fe^{2+} derived from the paramagnetic region above T_N was $5.0(1)\mu_B$. At fields >0.7 T, the antiferromagnetic phase is not observed, and a paramagnetic–ferrimagnetic (spin–flop) transition occurs at *ca.* 44 K. Fig. 4 shows the final refined magnetic structure. Tables 1–4 present the results of the two refinements; atomic positions, instrumental parameters and the bond distances and angles obtained from the 59.7(1) K data. Observed, calculated and difference profiles for the two temperatures are shown in Fig. 5. For clarity, the background has been subtracted from the normalised data and the nuclear peaks have been scaled to appear of equal height in each pattern.

Discussion

A number of magnetic exchange pathways are available for this structure, illustrated in Fig. 6, and the most probable of these will be discussed to ascertain the relative strengths of each type of interaction, and thus the structure-directing mechanism.

Table 1 Details of least-squares refinements from simultaneous Rietveld refinement of time-of-flight powder neutron data collected at the 153, 90 and 40° detector banks on HIPD

detector	no. data	no. refl.	wR_p (%)	R_p (%)	R_{exp} (%)	R_{nuc} (%)	R_{mag} (%)
(*a*) nuclear refinement at 59.7(1) K							
153°	5596	12610	3.82	2.64	2.92	3.11	–
90°	5226	2836	3.37	2.32	2.65	1.66	–
40°	3861	357	3.26	2.41	2.48	3.84	–
Reduced $\chi^2 = 1.69$ for 59 variables							
$a = 6.0186(4)$ Å; $b = 4.7768(3)$ Å; $c = 10.4192(8)$ Å; $\beta = 90.952(2)°$							
(*b*) nuclear and magnetic refinement at 10.1(1) K							
153°	4999	6154	4.01	2.73	3.24	3.11	10.26
90°	5223	3546	3.65	2.51	2.95	1.66	7.22
40°	5076	1063	4.00	2.83	3.15	3.84	3.08
Reduced $\chi^2 = 1.57$ for 57 variables							
$a = 6.0137(4)$ Å; $b = 4.7727(3)$ Å; $c = 10.4052(7)$ Å; $\beta = 90.944(2)°$							

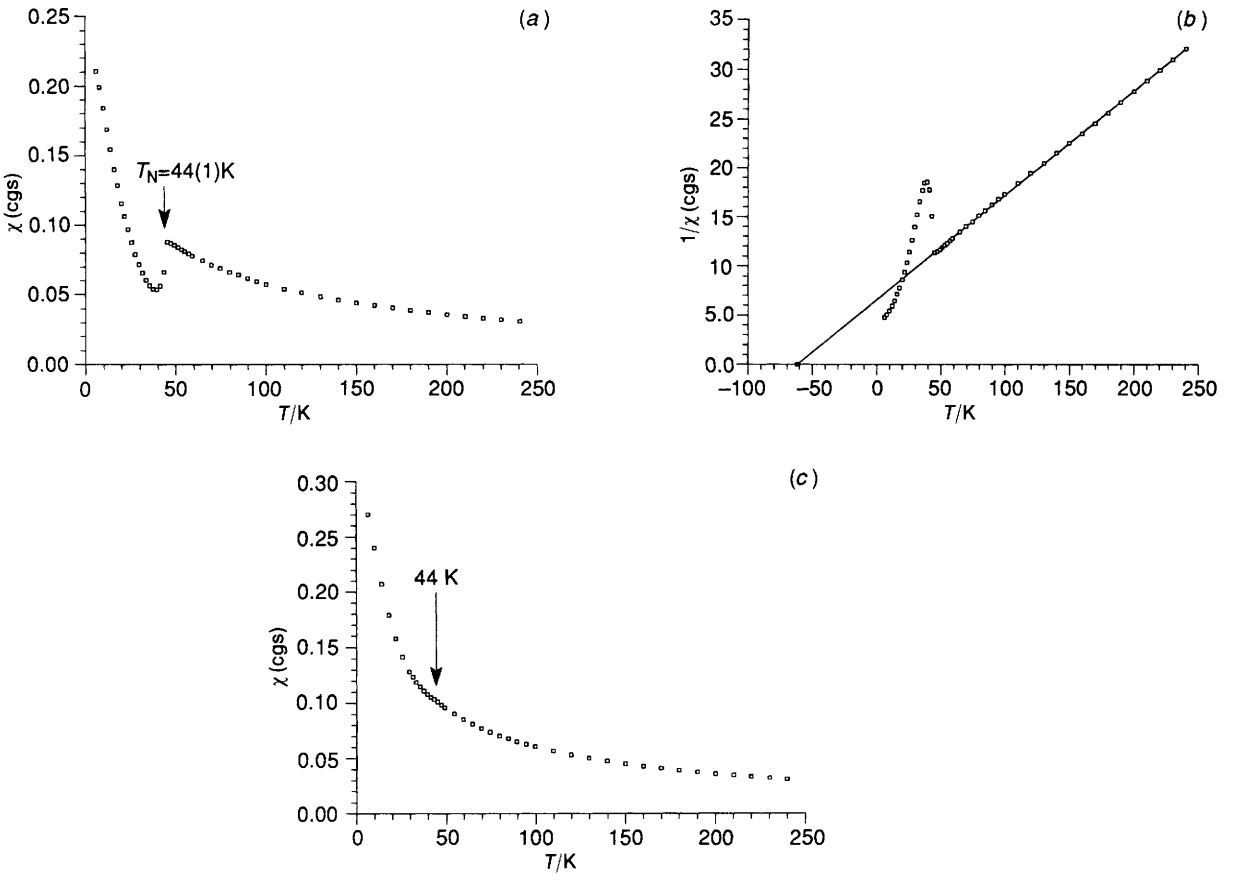

Fig. 3 (*a*) Susceptibility data collected on $Fe_3(PO_4)_2$, sarcopside, at 0.005 T from 6 to 240 K using a SQUID susceptometer. (*b*) Inverse susceptibility at 0.005 T showing extrapolation of the paramagnetic component [Fe^{II} moment = 5.0(1) μ_B] to the Weiss temperature at −67(2) K. (*c*) Susceptibility at 0.7 T showing the paramagnetic to spin–flop transition at *ca.* 44 K

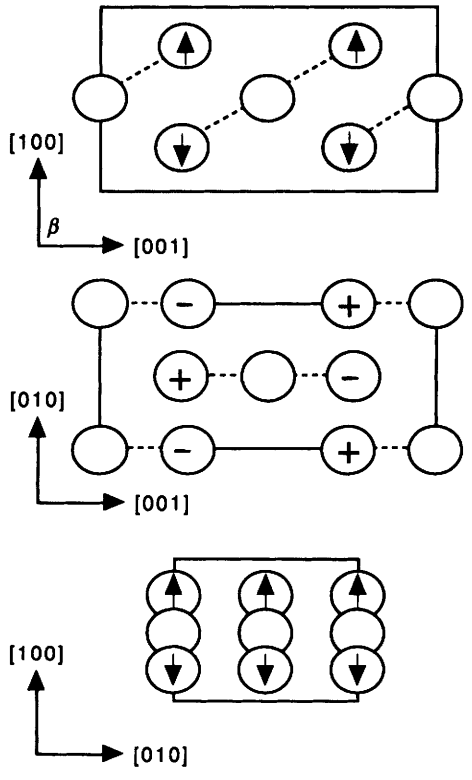

Fig. 4 Schematic projection of the magnetic structure of $Fe_3(PO_4)_2$, sarcopside, viewed down the [010], [100] and [001] axes. The dotted lines connect the iron sites within edge-sharing octahedra

Table 2 Atomic coordinates obtained for $Fe_3(PO_4)_2$, sarcopside, at (*a*) 59.7 and (*b*) 10.1 K

atom		*x*	*y*	*z*	U_{iso}/Å^2
M(1)	(*a*)	0.5	0	0	0.0020(2)
	(*b*)	0.5	0	0	0.0019(3)
M(2)	(*a*)	0.2372(2)	−0.0158(2)	0.2822(1)	0.0016(2)
	(*b*)	0.2375(2)	−0.0152(2)	0.2821(1)	0.0012(2)
P	(*a*)	0.2602(3)	0.4330(3)	0.1004(2)	0.0027(3)
	(*b*)	0.2602(3)	0.4327(3)	0.1005(2)	0.0022(3)
O(1)	(*a*)	0.2777(3)	0.7546(2)	0.1042(2)	−0.0005(2)
	(*b*)	0.2778(3)	0.7547(2)	0.1042(2)	0.0015(3)
O(2)	(*a*)	0.2531(3)	0.1797(3)	0.4640(1)	0.0025(3)
	(*b*)	0.2533(3)	0.1810(3)	0.4638(1)	0.0021(3)
O(3)	(*a*)	0.0719(2)	0.3250(3)	0.1821(2)	0.0015(3)
	(*b*)	0.0716(2)	0.3245(3)	0.1820(2)	0.0019(3)
O(4)	(*a*)	0.4684(2)	0.2851(3)	0.1624(2)	0.0030(3)
	(*b*)	0.4680(3)	0.2852(3)	0.1627(2)	0.0024(3)

(i) M(1)–M(2) *cation–cation interactions.* When the octahedra surrounding two neighbouring cations share a common edge, exchange between their t_{2g} d orbitals is possible. The strength of this effect is greatest when the t_{2g} orbitals are half filled, e_g orbitals are empty and the distance between the cations is small.[19] In this structure the intercation distance is relatively large {*d*[M(1)–M(2)] = 3.362(2) Å} and the e_g orbitals are half filled; thus the interaction is predicted to be rather weak and antiferromagnetic.[20]

(ii) M(1)–M(2) *superexchange.* The half-filled, anion-directed e_g orbitals can undergo spin transfer through the oxygen pσ and pπ orbitals.[20,21] This mechanism is expected to be weak as the angles involved are 103.98(2)° *via* O(1) and 114.59(7)°

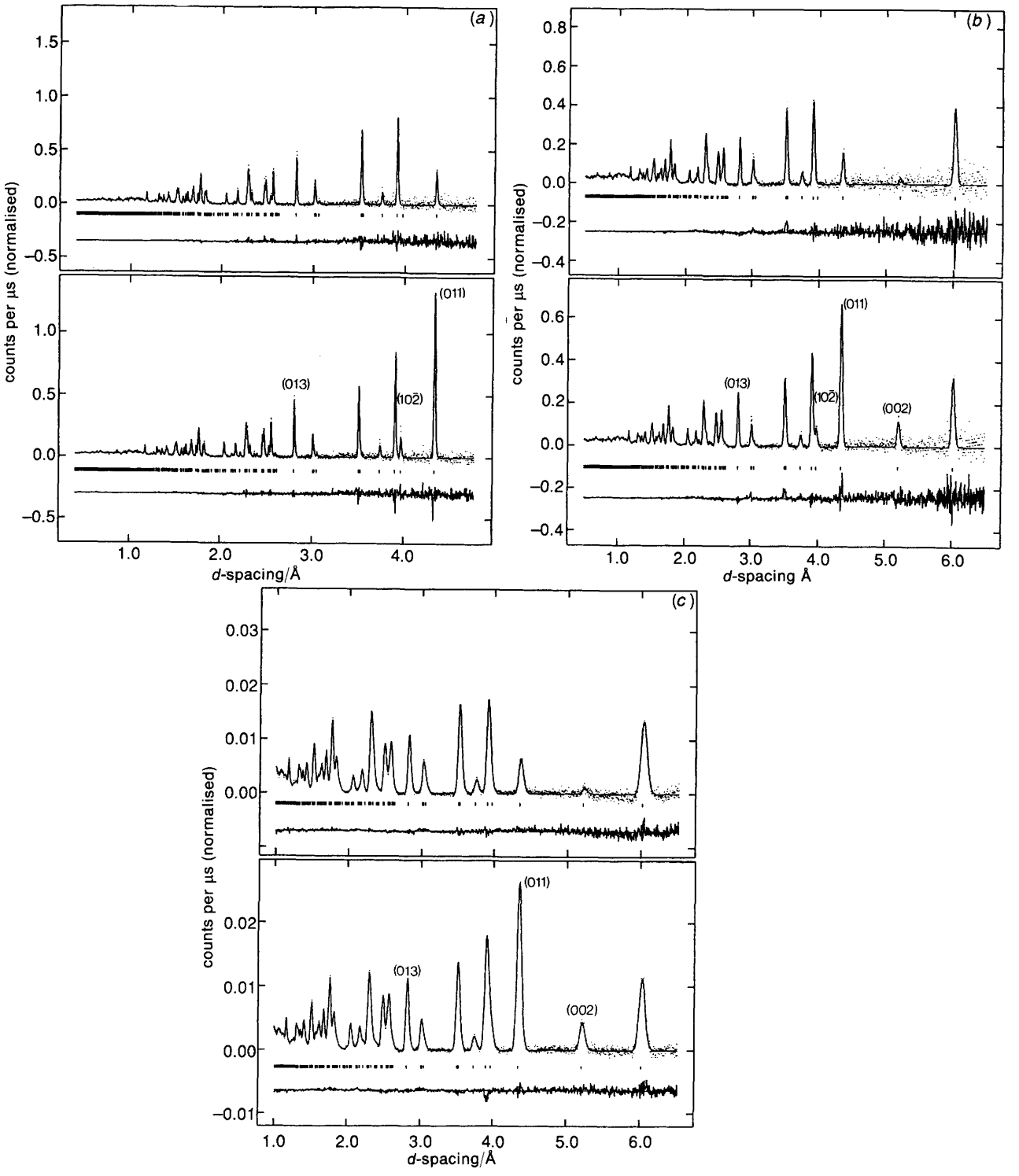

Fig. 5 Observed (dots), calculated (full line) and difference normalised time-of-flight, neutron diffraction profiles at 59.7 K and 10.1 K, from data collected at (i) 153, (ii) 90 and (iii) 40 ° detector banks on HIPD. The reflection markers are shown as bars and the principal magnetic peaks have been labelled. The background has been subtracted

via O(4). The strength of the exchange decreases rapidly as the angle deviates from 90° and the orbital overlap is reduced. d^6–d^6 90° cation–anion–cation superexchange is predicted to be weakly ferromagnetic.[20]

(iii) M(2)–M(2) *interchain superexchange*. Antiferromagnetic ordering occurs between M(2) sites in different chains *via* O(3). The M(2)–O(3)–M(2) angle of 127 ° allows the strong antiferromagnetic interaction predicted for 180° superexchange to dominate over the weaker ferromagnetic 90° mechanism.

(iv) M(2)–M(2) *intrachain superexchange*. The pathways through M(2)–O–M(1)–O–M(2) have a rather large through-bond length [8.55(1) Å], and will result in very weak ferromagnetic interactions between M(2) sites. Two symmetric M(2)–O(2)–P–O(3)–M(2) pathways [7.20(1) Å] related by the inversion centre link the M(2) sites at either end of a chain. As this configuration is almost planar, antiferromagnetic exchange between the d orbitals on M(2) through the molecular orbitals of the phosphate group will be stronger. This

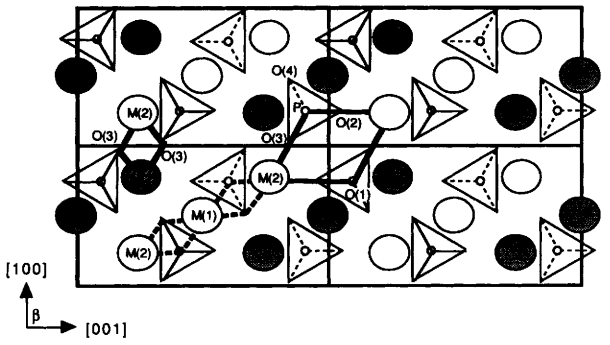

Fig. 6 Possible superexchange pathways in $Fe_3(PO_4)_2$, sarcopside. Phosphorus atoms within the oxygen tetrahedra are shown as small white circles. The large circles represent Fe sites, with the chains depicted in grey and white as *ca.* $y=0$ and $y=0.5$, respectively. The thick solid lines are used for intra- and inter-chain paths between M(2) sites, and the paths between M(1) and M(2) sites are shown with a thick dashed line

Table 3 Refined instrumental parameters for each detector bank at (*a*) 59.79(1) and (*b*) 10.1 K

	153°	90°	40°
scale (*a*)	1.08(1)	1.17(1)	1.19(1)
(*b*)	0.881(3)	0.949(2)	0.946(2)
absorption (*a*)	−0.036(1)	−0.047(1)	−0.029(2)
(*b*)[b]	−0.036	−0.047	−0.029
peak shape (σ^1) (*a*)	65(1)	170(2)	122(1)
(*b*)	64(1)	170(2)	120(1)
difA (*a*)	−2.75(12)	−2.18(8)	−0.96(3)
(*b*)	−2.13(10)	−1.76(7)	−1.31(3)
zero (*a*)	−0.7(3)	−3.7(2)	−8.9(2)
(*b*)	0.6(3)	−3.1(2)	−11.2(2)
back 1[a] (*a*)	0.0484(4)	0.0692(6)	−0.0354(2)
(*b*)	0.0337(3)	0.0458(4)	0.0385(4)
back 2 (*a*)	−0.0137(6)	−0.0391(9)	0.0698(1)
(*b*)	−0.0055(5)	−0.0199(7)	−0.0052(7)
back 3 (*a*)	0.0026(5)	0.0118(7)	−0.0458(8)
(*b*)	0.0023(4)	0.0072(6)	−0.0048(6)
back 4 (*a*)	−0.0002(4)	−0.0063(5)	0.0190(9)
(*b*)	−0.0001(3)	−0.0029(4)	0.0019(4)
back 5 (*a*)	0.0059(2)	0.0074(2)	−0.0045(4)
(*b*)	0.0043(2)	0.0048(2)	−0.0021(2)

Neutron scattering lengths from Koster and Yelon.[25] [a] A cosine Fourier series background function. [b] Fixed to avoid excessive correlation with the refined magnetic moment.

effect may be further enhanced since the P–O distances of the participating bonds are significantly shorter than the others and the angle is close to the tetrahedral angle.[22] Weak Fe–O–P–O–Fe superexchange has been studied by Battle *et al.*[23] in $KBaFe_2(PO_4)_3$ between 4.2 and 3.9 K. Stronger interactions have been observed in $NaFeP_2O_7$,[4,7] and in $Na_3Fe_2(PO_4)_3$,[3] where the FeO_6 octahedra are linked by PO_4 tetrahedra, with Néel temperatures of 29 and 47 K, respectively.

To understand the observed ordering (+0−) within the chains, the antiferromagnetic interactions between M(2) sites must be dominant. Weak interactions through the phosphate group, coupled with the stronger inter-chain superexchange between M(2) sites would explain the frustration of the moment on M(1) which has no net spin direction owing to the highly symmetric magnetic field. This can be rationalised crystallographically, as the centre of inversion at this site allows two possibilities for the magnetic moment, either zero or the full moment depending upon the magnetic symmetry. To maintain the same reflection conditions as the nuclear structure ($P2_1/c$) and provide a collinear antiferromagnetic arrangement of the spins, the magnetic structure must possess an anti-inversion centre. Our model requires the application of time reversal to the symmetry operator related to the *c* glide. Under these conditions (magnetic space group $P2_1/c'$), the spin contribution from each operator would cancel at the M(1) site. This reflects the observed paramagnetic moment on M(1), which has no net spin direction in the absence of an applied field, owing to frustration.

Although the lack of spin ordering on the M(1) site is an unusual result, it is consistent with a Mössbauer study[24] of this material at 5.2 K which found that whilst the signal from the M(2) site is magnetically ordered, the M(1) cation is paramagnetic. In the Mössbauer spectrum at 1.6 K, the paramagnetic M(1) doublet is decreased by 40%, indicating a second magnetic transition below 2.4 K.

The magnetic susceptibility measurements indicate a ferrimagnetic transition at 44 K. A ferromagnetic component could not be successfully incorporated into our model using the neutron data, and we feel that the ferrimagnetism observed at 10 K in the susceptibility data may be due to a spin–flop phase transition induced by the field in the SQUID, or indicate the lack of sensitivity of the neutron experiment, which is limited by the resolution and nature of the powder data. A single-crystal neutron study of this material, and particularly its field-dependent effects, would be of great interest.

Table 4 Interatomic distances and angles in $Fe_3(PO_4)_2$, sarcopside at 59.7 K

atoms	distances/Å	atoms	angle/degrees
M(1)—O(1) (×2)	2.095(2)	O(1)—M(1)—O(2′)	87.55(5)
M(1)—O(2′) (×2)	2.161(2)	O(1)—M(1)—O(4)	96.73(5)
M(1)—O(4) (×2)	2.183(2)	O(4)—M(1)—O(2′)	67.94(5)
M(1)—M(2)	3.363(2)	O(2)—M(2)—O(3)	91.66(7)
		O(2)—M(2)—O(4)	85.86(6)
		O(3)—M(2)—O(4)	123.42(8)
M(2)—O(1)	2.172(2)	M(2)—O(3)—M(2)[a]	127.21(8)
M(2)—O(2)	2.113(2)	M(1)—O(4)—M(2)	114.49(8)
M(2)—O(3)	2.050(2)	M(1)—O(1)—M(2)	104.00(6)
M(2)—O(3″)	2.166(2)	M(2)—O(2)—P‴	132.99(9)
M(2)—O(4)	2.084(2)	M(2)—O(3)—P	131.58(10)
M(2)—O(4″)	2.370(2)		
		O(1)—P—O(2′)	112.2(1)
		O(1)—P—O(3)	112.1(1)
P—O(1)	1.540(2)	O(1)—P—O(4)	112.6(1)
P—O(2′)	1.519(2)	O(2′)—P—O(3)	113.3(1)
P—O(3)	1.519(2)	O(2′)—P—O(4)	103.6(1)
P—O(4)	1.569(2)	O(3)—P—O(4)	102.4(1)

[a] Interchain connection; [b] symmetry transformations: ′ x, $1/2-y$, $1/2+z$, ″ $-x$, $1/2+y$, $1/2-z$, ‴ $-x$, $-y$, $-z$.

References

1 C. Gleitzer, *Eur. J. Solid State Inorg. Chem.*, 1991, **28**, 77.
2 A. Modaressi, J. C. Kaell, B. Malaman, R. Gerardin and C. Gleitzer, *Mater. Res. Bull.*, 1983, **18**, 101.
3 D. Beltran-Porter, R. Olazcuaga, L. Fournes, F. Menil and G. Le Flem, *Rev. Phys. Appl.*, 1980, **15**, 1155.
4 T. Moya-Pizzaro, R. Salmon, L. Fournes, G. Le Flem, B. Wanklyn and P. Hagenmuller, *J. Solid State Chem.*, 1984, **53**, 387.
5 P. D. Battle, A. K. Cheetham, C. Gleitzer, W. T. A. Harrison, G. J. Long and G. Longworth, *J. Phys. C: Solid State Phys.*, 1982, **15**, L919.
6 A. Modaressi, A. Courtois, R. Gerardin and C. Gleitzer, *J. Solid State Chem.*, 1983, **47**, 245.
7 R. C. Mercader, L. Terminiello, G. J. Long, D. G. Reichel, K. Dickhaus, R. Zysler, R. Sanchez and M. Tovar, *Phys. Rev.*, **B42**, 25.
8 J. K. Warner, A. K. Cheetham, D. E. Cox and R. B. Von Dreele, submitted.
9 M. Ijjaali, B. Malaman, C. Gleitzer, J. K. Warner, J. A. Hriljac and A. K. Cheetham, *J. Solid State Chem.*, 1990, **86**, 195.
10 E. Kostiner and J. R. Rea, *Inorg. Chem.*, 1974, **13**, 2876.
11 P. B. Moore, *Am. Mineral.*, 1972, **57**, 24.
12 O. V. Yakubovich, E. L. Belokoneva, V. G. Tsirel'son and V. S. Urusov, *Bull. Moscow Univ. Sect. 4; Geology*, 1991, **2**, 88.
13 C. Calvo and R. Faggiani, *Can. J. Chem.*, 1975, **53**, 1516.
14 T. Ericsson and A. G. Nord, *Am. Mineral.*, 1984, **69**, 889.
15 H. M. Rietveld, *J. Appl. Crystallogr.*, 1969, **2**, 65.
16 A. C. Larson and R. B. Von Dreele, Los Alamos National Laboratory *Rep. No. LA-UR-86-748*, 1987.
17 E. Clementi and C. Roetti, *Atomic Data and Nuclear Data Tables*, 1974, **14**, 177.
18 P. J. Brown and J. C. Matthewman, *Rutherford Appleton Research Laboratories Rep.*, RAL-87-010, 1987.
19 J. B. Goodenough, *J. Appl. Phys.*, 1960, **31S**, 359.
20 J. B. Goodenough, *Magnetism and the Chemical Bond*, Wiley, New York 1963, pp. 165–190.
21 J. Kanamori, *J. Phys. Chem. Solids*, 1959, **10**, 87.
22 P. W. Anderson, in *Magnetism*, Ed. G. Rado and H. Suhl, Academic Press, 1963, vol. 1, p. 25.
23 P. D. Battle, A. K. Cheetham, W. T. A. Harrison and G. L. Long, *J. Solid State Chem.*, 1986, **62**, 16.
24 T. Ericsson and F. Khangi, *Hyperfine Interactions*, 1988, **41**, 783.
25 L. Koster and W. B. Yelon, *Summary of Low Energy Neutron Scattering Wavelengths and Cross-Sections*, Netherlands Energy Research Foundation, Department of Physics, Petten, 1982.

Paper 1/04195I; *Received* 12*th August*, 1991